ELSEVIER

Journal of Power Sources 81–82 (1999) 212–216

JOURNAL OF POWER SOURCES

www.elsevier.com/locate/jpowsour

In situ investigation of the interaction between graphite and electrolyte solutions

Petr Novák *, Felix Joho, Roman Imhof [1], Jan-Christoph Panitz, Otto Haas

Paul Scherrer Institute, Electrochemistry Section, CH-5232 Villigen PSI, Switzerland

Abstract

The formation of a solid electrolyte interphase (SEI) before and during lithium intercalation was studied on graphite electrodes in ethylene carbonate based electrolytes. We demonstrated by using in situ mass spectrometry that during the first charge of the graphite electrode ethylene gas is evolved in a potential window that corresponds to the formation of a SEI. Moreover, development of hydrogen gas was detected even in dry electrolytes containing < 10 ppm H_2O. No CO_2 is developed however, as confirmed by two in situ methods, mass spectrometry and infrared spectroscopy. We conclude that the formation of the SEI is a complex process which depends among other things on the amount of trace water present in the cell. In addition, in situ Raman mapping experiments revealed that lithium intercalation into graphite does not proceed homogeneously.

Keywords: Lithium-ion cell; Graphite electrode; SEI-film; Electrolyte decomposition; In situ mass spectrometry; In situ infrared spectroscopy; In situ Raman mapping

1. Introduction

Carbon-based negative electrodes are widely used in combination with lithium-containing positive electrodes as components in lithium-ion batteries having high energy density and good cycleability [1]. However, understanding the irreversible charge loss occurring during the first charging of carbon electrodes is still a challenge. It is generally accepted that this charge loss is mainly due to the reductive decomposition of the electrolyte on the negative electrode. As a result of this decomposition a protective film called the solid electrolyte interphase (SEI) is formed that allows Li^+-ion transfer but prevents electron transfer. The SEI formation mechanism is complex and is not yet completely understood (for recent reviews see Refs. [2,3]). In this work the SEI formation before and during lithium intercalation is studied on graphite electrodes in ethylene carbonate based electrolytes using several in situ methods.

2. Experimental

The experiments were performed at room temperature using a 1 M solution of $LiClO_4$ (Merck) in a 1:1 (v/v) mixture of ethylene carbonate (EC, Merck) and dimethyl carbonate (DMC, Merck). The water content of this standard electrolyte was determined to be about 8 ppm by Karl–Fischer titration. Lithium metal was used as the counter and reference electrodes. All potentials throughout the paper are reported with reference to the Li/Li^+ couple.

Galvanostatic charge/discharge experiments were performed in laboratory cells described elsewhere [4]. Working electrodes were prepared from the synthetic graphites TIMREX® SFG 44 and SFG 6 (TIMCAL, Switzerland), respectively. A slurry of graphite suspended in a solution of poly(vinylidene fluoride) (PVDF) in 1-methyl-2-pyrrolidone was sprayed on a thick stainless steel current collector and then dried under vacuum at 120°C overnight. The electrodes contained ca. 8 mg cm^{-2} of graphite and 5 wt.% of PVDF binder. They were galvanostatically cycled at a rate of 10 $\mu A\ mg^{-1}$ of graphite between 1500 and 5 mV vs. Li/Li^+. At 5 mV the specific current was lowered potentiostatically to $\leq 5\ \mu A\ mg^{-1}$.

* Corresponding author. Tel.: +41-56-310 2457; Fax: +41-56-310 4415; E-mail: petr.novak@psi.ch

[1] Present address: Renata AG, CH-4452 Itingen, Switzerland.

0378-7753/99/$ - see front matter
PII: S0378-7753(99)00119-6

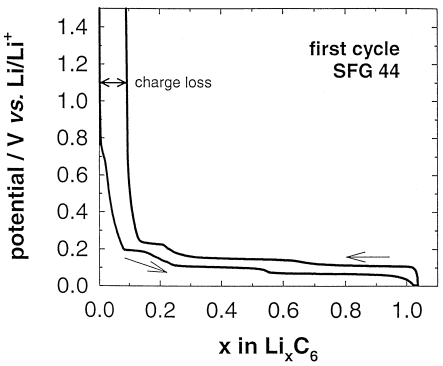

Fig. 1. Galvanostatic charge/discharge curve of a graphite SFG 44 electrode.

Differential electrochemical mass spectrometry (DEMS) was used for the identification of gaseous and volatile products evolved at the graphite electrode during cycling, as described in Refs. [5,6]. SFG 6 was the active material of the working electrode containing 5 wt.% of PVDF as binder. The electrode was mechanically supported by a porous GORE-TEX® ePTFE pV 9008 membrane. The measurements were carried out potentiodynamically with a scan rate of 0.4 mV s^{-1}. The current (CV) together with the mass signals (MSCV) were recorded simultaneously as a function of potential.

In situ infrared experiments were performed in the SNIFTIRS mode (subtractively normalized interfacial fourier transform infrared spectroscopy) [7]. The setup is described in Refs. [8,9]. The potential-dependent changes at the electrode/electrolyte interface and/or in the thin electrolyte layer between the electrode and the optical window (CaF_2) are visualized by plotting R/R_0, where R is the reflectance single beam spectrum taken at the working electrode potential and R_0 the background single beam spectrum taken at the open circuit potential. The working electrode was a mechanically polished glassy carbon (GC) disc. It was covered by spraying with a thick layer of graphite SFG 6 with 10 wt.% of PVDF as binder. The surface of the graphite was gently smoothed out with a sheet of paper. The spectra R were measured at a resolution of 4 cm^{-1} by accumulating 128 scans during a potential scan at 0.4 mV s^{-1}. The measuring time of each spectrum R was about 5 min with a DTGS detector.

In situ Raman spectroscopy was performed with a confocal Raman microscope (LabRam, DILOR/Instruments) using the 530.901 nm line of an external Kr^+ ion laser in a specially constructed spectro-electrochemical cell [10]. By using a microscope with an ultralong working distance objective (Olympus) with a 50 × magnification it is possible to obtain Raman spectra from a depth of up to 4 mm below the sapphire optical window. With the pinhole diameter adjusted to 200 μm the lateral resolution is 4 μm according to the manufacturer's specification. The laser power was adjusted to 3–4 mW in order to avoid damage to the electrode surface. The working electrode consisted of the graphite SFG 44 with 5 wt.% PVDF as binder. During the collection of the Raman spectra the electrode was galvanostatically cycled at a rate of ca. 100 μA mg^{-1} of graphite in a potential window from 1500 to 5 mV vs. Li/Li^+. For the mapping routine the current was interrupted and the mapping was performed at a constant potential.

3. Results and discussion

3.1. Galvanostatic charge / discharge experiments

Fig. 1 shows the first galvanostatic charge/discharge curve of the graphite SFG 44. The charge consumed due to side reactions in the first cycle (in technical literature frequently called the 'charge loss') is clearly visible. The charge loss is generally ascribed to electrolyte decomposition and corrosion-like reactions of Li_xC_6 which both form the SEI [2,3]. The SEI film is composed of alkyl carbonates, Li_2CO_3, and salt reduction products (e.g., LiCl from $LiClO_4$) [11]. According to Aurbach et al. [12], 1.5 V vs. Li/Li^+ may be considered as the onset potential for the salt reduction. However, only little faradaic current flows in the whole potential region positive to about 800 mV. Thus, SEI is mainly formed in the potential region negative to about 800 mV vs. Li/Li^+ as indicated by the

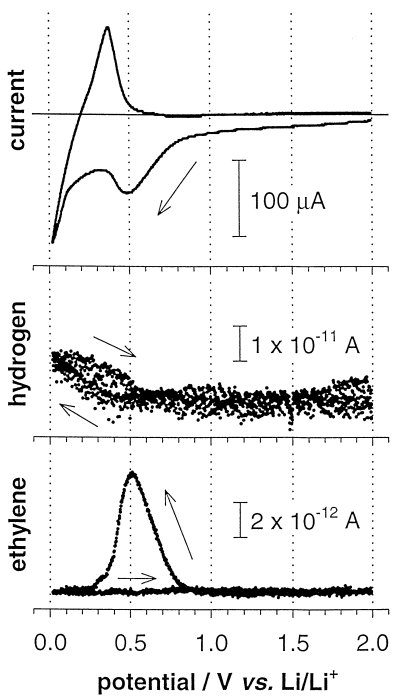

Fig. 2. CV (above) and two MSCV's (middle and below) of a graphite SFG 6 electrode (first cycle). The MSCV's show $m/z = 2$ and $m/z = 27$, representing hydrogen and ethylene, respectively. (Consider that the measurements were performed at a relatively high scan rate of 0.4 mV/s. Thus, the coulombic efficiency of lithium insertion/extraction is rather low in comparison to experiments discussed in literature.)

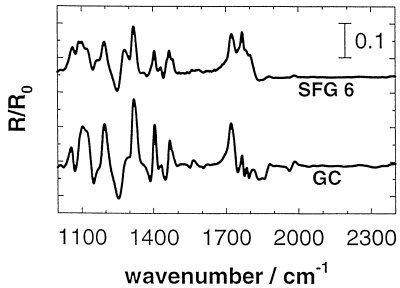

Fig. 3. SNIFTIR spectra measured from 400 mV to 272 mV vs. Li/Li^+ at a graphite electrode (SFG 6) and a polished glassy carbon (GC) electrode.

distinct sloping potential plateau in Fig. 1. Our experiments revealed that the electrochemical properties of both graphite types used in this study are similar except for the charge loss in the first cycle which is ~10% for SFG 44 and ~20% for SFG 6. This difference can be explained with the different BET specific surface area of the samples (SFG 6: 15.2 $m^2\ g^{-1}$; SFG 44: 4.3 $m^2\ g^{-1}$) as discussed elsewhere [13].

3.2. In situ mass spectrometry

In situ mass spectrometric experiments on graphite electrodes revealed that both ethylene and hydrogen gas are formed in EC containing electrolytes [5,6]. No other volatile products were detected. The ethylene evolution is restricted (i) to the first charging half-cycle and (ii) to a potential window from ~800 to ~200 mV vs. Li/Li^+. The mass signals of the ethylene fragments correlate well with a negative current peak in the cyclic voltammogram which corresponds to the formation of the SEI (Fig. 2). Our results seem to contradict other studies on *complete cells* where besides ethylene mainly CO but also other species such as methane, ethane, and CO_2 have been collected and identified [14–16]. This difference might be related to the fact that only gases which are evolved at the working electrode are analyzed in our DEMS experiments.

For supplementary measurements water was added to the standard electrolyte. Then, a series of DEMS experiments was performed for water contents from 10 to 4000 ppm H_2O. As already shown in Ref. [5] and further elaborated in a related paper in this volume [17], the more trace water the electrolyte contains, the less ethylene is evolved. In wet electrolytes hydrogen gas from water reduction can be detected at potentials negative to ~1300 mV vs. Li/Li^+. Hydrogen evolution was also detected in the dry electrolyte (< 10 ppm H_2O) but only at potentials negative to ~600 mV vs. Li/Li^+ (Fig. 2). In contrary to ethylene, this hydrogen mass signal appears with about the same intensity also in the second cycle. The hydrogen source has not been identified yet. (Be aware that the reduction of both water and organic material is possible.)

3.3. In situ infrared spectroscopy

To confirm the absence of CO_2 by an independent method in situ infrared spectroscopic experiments were performed. Two representative spectra are shown in Fig. 3. The interpretation of the spectral bands below 2000 cm^{-1} is difficult because the spectra of the reaction products coincide with the spectra of the bulk electrolyte. Nevertheless, the absence of a CO_2 absorption band expected at 2342 cm^{-1} (and detected with the same setup in another electrolyte system [18]) clearly proves that no CO_2 is generated during the SEI formation in the EC + DMC electrolyte. Furthermore, despite the different lithium intercalation behavior of GC and graphite in non-aqueous electrolytes, the similarity of the two infrared spectra indicates that a GC electrode can be used as a model surface for the infrared spectroscopic investigation of the SEI formation on carbon. A detailed examination of in situ infrared spectra acquired at GC electrodes in EC + DMC electrolyte solutions containing $LiClO_4$, $LiPF_6$, and $LiN(SO_2CF_3)_2$, respectively [5], revealed that the concentration of the electrolyte salt anions near the electrode surface decreases in the potential range where the SEI is formed.

All the mentioned observations allow us to conclude that the formation of the SEI is a complex process which depends among other things on the amount of trace water present in the cell. The absence of species like C_2H_6 and CO_2 makes some of the SEI formation mechanisms suggested in the recent literature [19,20] less probable. Scheme 1 summarizes the reactions which are compatible with our experiments.

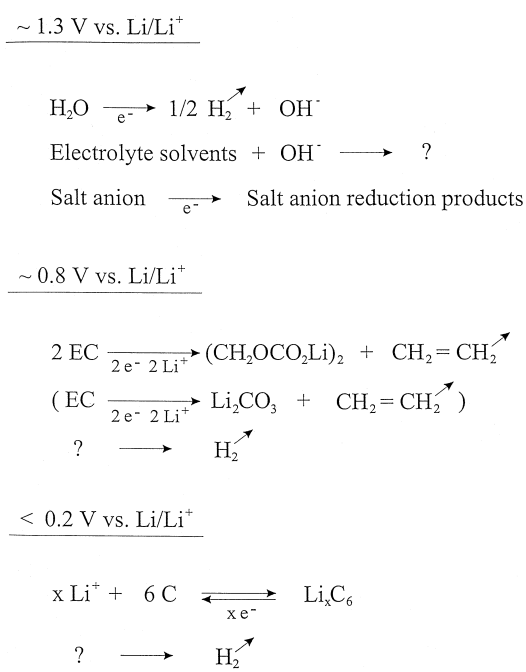

Scheme 1. Possible reactions occurring on the graphite electrode during the first charging half-cycle.

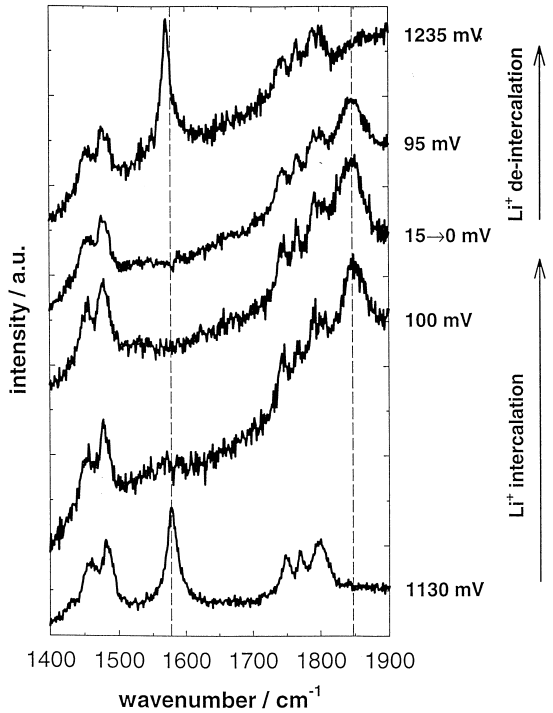

Fig. 4. In situ Raman spectra measured at the electrode surface at indicated potentials during the first intercalation/de-intercalation process of a graphite SFG 44 electrode.

3.4. In situ Raman microscopy

Additional information can be obtained from in situ Raman microscopy. Our measurements performed during the first lithium intercalation/de-intercalation cycle confirmed the published results [21,22]. In addition, a new band at ca. 1850 cm^{-1} was detected at potentials more negative than $\sim$160 mV vs. Li/Li^+ upon first lithium intercalation (Fig. 4). We like to point out that this band is only observed very close to the electrode surface. It reaches the strongest intensity when LiC_6 is formed at potentials close to 5 mV vs. Li/Li^+. Upon lithium de-intercalation, the intensity of the band decreases but it remains clearly detectable up to a potential of $\sim$800 mV. It nearly vanishes at more positive potentials however (Fig. 4). A tentative explanation for this band is the formation of complexes between Li^+ and EC and/or its decomposition products. Another possible interpretation is associated with the observation of short-range orientation effects in liquid EC [23], which may be amplified at higher lithium ion concentrations. We have demonstrated elsewhere [10] that the Raman bands of EC change with changing lithium ion concentration. An extensive discussion of the band at ca. 1850 cm^{-1} can be found in Ref. [10].

Furthermore, a negative shift of the Raman band related to the vibrations of lithium-free graphene layers [24] from ca. 1578 cm^{-1} to ca. 1571 cm^{-1} was noticed after the first lithium intercalation/de-intercalation cycle (Fig. 4). This indicates that the spectroscopic properties of the graphite changed during the electrochemical cycle.

Finally, in situ Raman mapping experiments were performed at several potentials during two cycles on real graphite electrodes. Both, the position and the intensity of the graphite-related bands in the region at about 1580

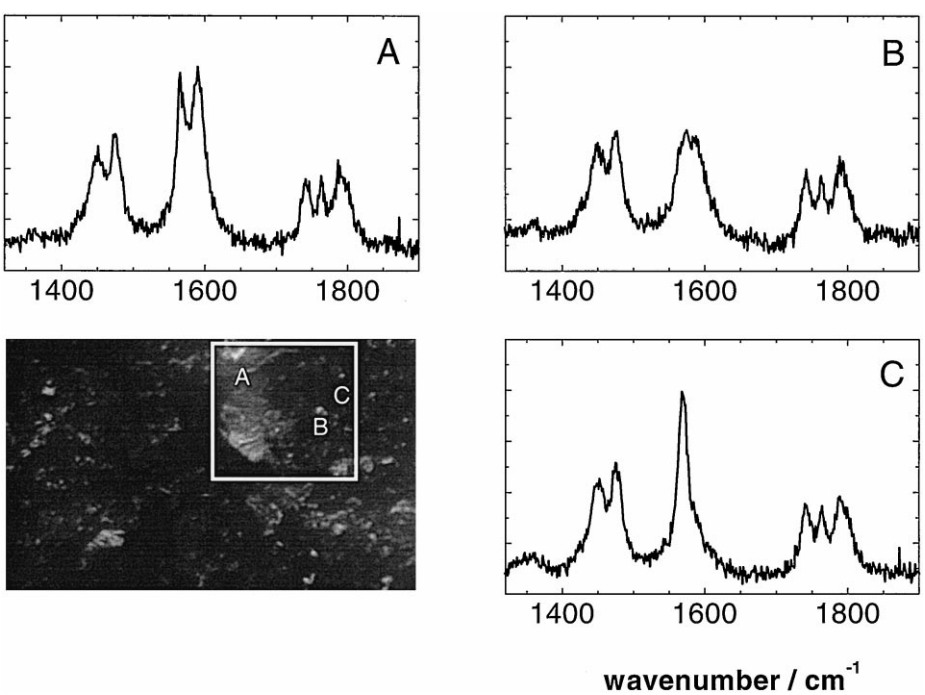

Fig. 5. In situ Raman spectra measured at the electrode surface at a constant potential of 200 mV vs. Li/Li^+ during the second reductive charging of a graphite SFG 44 electrode. Raman mapping was performed on an area of 50×50 μm marked with a white square in the picture from an optical microscope. The letters A, B, and C indicate the places where the shown spectra were measured.

cm^{-1} depend on the degree of lithium intercalation [21,22]. Thus, the intercalation stages of Li_xC_6 can be distinguished on a micrometer scale with Raman mapping. As shown in Fig. 5 the lithium intercalation does not proceed homogeneously at different sites on the electrode surface.

4. Conclusions

It follows from the in situ experiments that the formation of the SEI is a complex process which depends among other things on the amount of trace water present in the cell. We detected no CO_2 production during the SEI formation. We, therefore, think that more care has to be taken in applying some of the models suggested in the literature to discuss this complex process. Besides, the lithium intercalation into graphite does not proceed homogeneously.

Acknowledgements

This work was supported by the Swiss Federal Office of Energy, Bern. TIMCAL, Sins provided the graphite samples. We thank B. Rykart and Ch. Marmy for technical assistance and Dr. H.-P. Brack for critical reading of the manuscript.

References

[1] J.R. Dahn, A.K. Sleigh, H. Shi, B.M. Way, W.J. Weydanz, J.N. Reimers, Q. Zhong, U. von Sacken, in: G. Pistoia (Ed.), Lithium Batteries: New Materials, Developments and Perspectives, Elsevier, Amsterdam, 1994, p. 1.
[2] Z. Ogumi, M. Inaba, Bull. Chem. Soc. Jpn. 71 (1998) 521.
[3] M. Winter, J.O. Besenhard, M.E. Spahr, P. Novák, Adv. Mater. 10 (1998) 725.
[4] P. Novák, W. Scheifele, F. Joho, O. Haas, J. Electrochem. Soc. 142 (1995) 2544.
[5] R. Imhof, P. Novák, J. Electrochem. Soc. 145 (1998) 1081.
[6] R. Imhof, P. Novák, in: C.F. Holmes, A.R. Landgrebe (Eds.), Proceedings of the Symposium on Batteries for Portable Applications and Electric Vehicles, PV 97-18, The Electrochemical Society Proceedings Series, Pennington, NJ, 1997, p. 313.
[7] P.A. Christensen, A. Hamnett, in: R.G. Compton, A. Hamnett (Eds.), Chemical Kinetics: New Techniques for the Study of Electrodes and Their Reactions, Elsevier, Amsterdam, Vol. 29, 1989, p. 1.
[8] M. Winter, P. Novák, J. Electrochem. Soc. 145 (1998) L27.
[9] F. Joho, PhD Thesis No. 11745, ETH Zurich, Switzerland, 1996.
[10] J.-C. Panitz, F. Joho, P. Novák, Appl. Spectrosc., submitted.
[11] D. Aurbach, B. Markovsky, A. Schechter, Y. Ein-Eli, H. Cohen, J. Electrochem. Soc. 143 (1996) 3809.
[12] D. Aurbach, O. Chusid, I. Weissman, P. Dan, Electrochim. Acta 41 (1996) 747.
[13] M. Winter, P. Novák, A. Monnier, J. Electrochem. Soc. 145 (1998) 428.
[14] A. Ohta, H. Koshina, H. Okuno, H. Murai, J. Power Sources 54 (1995) 6.
[15] A.S. Gozdz, R.K. Jaworski, Abstract 43, The Electrochemical Society Meeting Abstracts, Vol. 96-1, Los Angeles, CA, May 1996.
[16] H. Yoshida, T. Fukunaga, T. Hazama, M. Terasaki, M. Mizutani, M. Yamachi, J. Power Sources 68 (1997) 311.
[17] F. Joho, B. Rykart, R. Imhof, P. Novák, M.E. Spahr, A. Monnier, J. Power Sources 81–82 (1999) 243–247.
[18] M. Winter, R. Imhof, F. Joho, P. Novák, J. Power Sources 81–82 (1999) 818–823.
[19] M. Jean, A. Chaussé, R. Messina, Electrochim. Acta 43 (1998) 1795.
[20] C.R. Yang, Y.Y. Wang, C.C. Wan, J. Power Sources 72 (1998) 66.
[21] M. Inaba, H. Yoshida, Z. Ogumi, T. Abe, Y. Mizutani, M. Asano, J. Electrochem. Soc. 142 (1995) 20.
[22] W. Huang, R. Frech, J. Electrochem. Soc. 145 (1998) 765.
[23] G. Fini, P. Mirone, B. Fortunato, J. Chem. Soc. Faraday Trans. II 69 (1973) 1243.
[24] F. Tuinstra, J.L. Koenig, J. Chem. Phys. 53 (1970) 1126.